Ocean Science
Discussions

Open Access

Phase Synchronisation in the Kuroshio Current System

Ann Kristin Klose[1], René M. van Westen[2], and Henk A. Dijkstra[2,3]

[1]ICBM, Carl von Ossietzky University Oldenburg, Oldenburg, Germany
[2]Institute for Marine and Atmospheric research Utrecht, Department of Physics, Utrecht University, Utrecht, the Netherlands
[3]Center for Complex Systems Studies, Utrecht University, Utrecht, the Netherlands

Correspondence to: Henk Dijkstra <h.a.dijkstra@uu.nl>

Abstract. The Kuroshio Current System in the North Pacific displays path transitions on a decadal time scale. It is known that both internal variability involving barotropic and baroclinic instabilities and remote Rossby waves induced by North Pacific wind-stress anomalies are involved in these path transitions. However, the precise coupling of both processes and its consequences for the dominant decadal transition time scale are still under discussion. Here, we analyse the output of a
5   multi-centennial long high-resolution global climate model simulation and study phase synchronisation between Pacific zonal wind-stress anomalies and Kuroshio Current System path variability. We apply the Hilbert transform technique to determine the phase and find epochs where such phase synchronisation appears. The physics of this synchronisation is shown to occur through the effect of the vertical motion of isopycnals, as induced by the propagating Rossby waves, on the instabilities of the Kuroshio Current System.

10   **1   Introduction**

The Kuroshio Current System (KCS) in the North Pacific plays an important role in climate through its meridional heat transport (Hu et al., 2015). Variations in Kuroshio flow patterns generate persistent sea surface temperature (SST) anomalies which influence the atmospheric midlatitude circulation and storm-track activities (Taguchi et al., 2009). Understanding the processes determining the mean path of the Kuroshio Current and its low-frequency (interannual-to-multidecadal time scale)
15   variability are hence crucial for skillful prediction of KCS flow patterns and for determining the behaviour of the KCS under the increase of greenhouse gases and its implications for regional climate change (Wu et al., 2012).

Observations have shown that both the Kuroshio Current (KC) and the Kuroshio Extension (KE) as part of the KCS exhibit variations in their path (Taft, 1972). The KC switches between a typical Large Meander (tLM) and a Non-Large Meander (NLM) state (Kawabe, 1995) on a few years time scale. The NLM state is usually divided into the near-shore NLM (nNLM)
20   and an off-shore NLM (oNLM) depending on the path it follows over the Izu Ridge. The KE displays transitions between a so-called elongated and a contracted state (based on the path length over a specified longitudinal range) on decadal time scales (Qiu, 2002). An elongated (contracted) state is characterised by a higher (lower) level of eddy kinetic energy (Qiu and Chen, 2010) as well as a smaller (larger) eastward surface transport, a more southerly (northerly) KE path and a weaker (stronger) southern recirculation gyre (Qiu and Chen, 2005). The relationship between KC and KE paths was investigated in Sugimoto

and Hanawa (2011). When the KC takes a tLM or nNLM path, the KE tends to prefer a contracted state and when the KC is in an oNLM state, the KE favors an elongated state.

From a theoretical point of view, the central problem is to explain the KCS path variability using the building blocks of geophysical fluid dynamics. The existence of western boundary currents in the ocean (such as the Kuroshio and also the Gulf Stream) is well explained by the linear Sverdrup-Stommel-Munk model (Sverdrup, 1947; Stommel, 1948; Munk, 1950) although properties of the western boundary layer flow in this model depend on highly idealised parameterisations of lateral and bottom friction. To explain more detailed aspects of the western boundary currents, such as their volume transport and their path variability, nonlinear stratified extensions of this model are needed.

One piece of the KCS path variability puzzle is clearly the non-stationary atmospheric forcing of the ocean flow. There is wind-stress variability over the eastern Pacific related to the Pacific Decadal Oscillation (PDO) (Mantua et al., 1997) and the North Pacific Gyre Oscillation (NPGO) (Di Lorenzo et al., 2008). Wind-stress variations cause sea surface height (SSH) anomalies through Ekman dynamics, which propagate westward as baroclinic Rossby waves (Deser et al., 1999). Altimetry data show a coincidence of the arrival of these SSH anomalies in the Kuroshio region and the transition between the KE states (Ceballos et al., 2009; Qiu and Chen, 2010). Upon the arrival of negative SSH anomalies, the KE weakens and the path shifts southward. An intensified mesoscale eddy field results from the subsequent interaction with the underlying topography enhancing the strength of the southern recirculation gyre. A northward migration of the KE is induced by the arrival of positive SSH anomalies (Qiu and Chen, 2010).

Another piece of the puzzle is the strong internal (or intrinsic) variability which can be generated solely through mixed barotropic/baroclinic instabilities. Studies using a hierarchy (quasi-geostrophic, shallow-water and primitive equation) of models have indicated that low-frequency path variability (both in the KC and KE) can occur under a stationary wind forcing (Schmeits and Dijkstra, 2001; Pierini, 2006; Pierini et al., 2009; Pierini, 2014; Gentile et al., 2018). Results from models having a relatively high value of the lateral friction coefficient have indicated the successive (barotropic) instabilities which generate the path variability (Speich et al., 1995; Simonnet et al., 2005; Pierini et al., 2009) through oscillatory instabilities and global bifurcations. In models which also capture baroclinic instabilities, a collective interaction of the mesoscale eddies eventually leads to a so-called turbulent oscillator (Berloff et al., 2007) in which the KCS displays low-frequency variability.

Approaches on combining both forced and internal views have been made as an attempt to develop a more detailed theory explaining the path transitions of the KCS and its dominant decadal time scale in terms of the interaction between forced Rossby waves and the internal variability (including the mesoscale eddies). When linear models (such as quasi-geostrophic or shallow-water models) are subjected to non-stationary wind-stress forcing, no path transitions are found due to the interaction of the Rossby waves and the western boundary current (Qiu and Chen, 2010) so internal variability appears essential for KSC path variability. Using a non-linear shallow-water model, Pierini (2014) shows that the KE path length and the NPGO index to be very well correlated suggesting that the KE internal variability is excited and paced by the North Pacific wind-stress forcing.

During the last decade, also much has been learned from the analysis of simulations with high-resolution ocean general circulation models (OGCMs). The relevance of internal ocean variability in the climate system was demonstrated by comparing OGCM simulations under realistic and climatological annual cycle atmospheric forcing (Penduff et al., 2011; Sérazin et al.,

2018). Taguchi et al. (2007) present a hind cast simulation analysis of the OFES model and indicate that Rossby waves generated by mid-Pacific wind stress anomalies can induce internal variability of the KE. Recent studies of the mechanical energy balance for the KCS region in OGCMs (Sérazin et al., 2018), re-analysis (Yang et al., 2017) products (such as ECCO) and also altimetry observations (Wang et al., 2016; Ma, 2019) have shed light on the dominant energy transfer processes.

5 Through inverse cascading processes, eddies with time scales of a few months continually loose kinetic energy to motions on longer time scales (Sérazin et al., 2018). Wang et al. (2016) show that the barotropic energy conversion between mean flow and eddies is the main source of low-frequency KE variability and that baroclinic processes are relatively unimportant. Yang et al. (2017) also show that the barotropic kinetic energy transfer lags the NPGO index by about 2 years.

In this paper, we contribute to the understanding of the KCS path variability focussing on what we think is a missing piece
10 to reconcile the forced and internal views as sketched above: a phase synchronisation of the KCS variability with the zonal wind-stress variability in the North Pacific. As will be explained in more detail in Section 2 below, phase synchronisation is a fairly general mechanism where an external forcing is entrained into the behaviour of a chaotic dynamical system (Pikovsky et al., 2001). We will use here a 300-years control simulation of the Community Earth System Model (CESM, version 1.0.4) because one needs a relatively long (multi-centennial) simulation with a high-resolution global climate model to detect such a
15 decadal time scale phase synchronisation.

We start with describing the model data and methods of analysis in Section 2. Results of the analysis of the CESM output are presented in Section 3, where we first provide results of a model-observation comparison (Section 3.1) followed by the phase synchronisation results (Section 3.2) and the physical mechanism of this synchronisation (Section 3.3). We summarise and discuss our findings in the context of previous work in Section 4.

20 ## 2 Models and Methods

We analyse output from a 300-years control simulation of the CESM (version 1.0.4) as performed at SURFSara, the Academic Computer Centre in Amsterdam. In this control simulation (see also van Westen et al. (2018)) all the forcing fields such as CO_2, CH_4, solar forcing and aerosols are the ones from the year 2000 and repeated every year. The ocean component of CESM, the Parallel Ocean Program (POP), has a horizontal resolution of 0.1° on a curvilinear grid so that mesoscale eddies are
25 explicitly captured. The POP has 42 non-equidistant vertical layers where the highest vertical resolution is near the surface. The atmospheric component with 30 non-equidistant pressure levels and the land-surface component have a horizontal resolution of 0.5°.

2.1 Model validation

From the model output, we extracted monthly averaged fields of sea surface height (SSH), zonal and meridional wind stress,
30 ocean horizontal velocity fields, ocean temperature and ocean salinity. For analysis these fields were transformed onto a rect-angular grid with a horizontal resolution of 0.4° × 0.4°. Only the last 151 model years of the CESM output (model years 150

– 300) are considered in the analysis because the upper ocean quantities are not in equilibrium yet during the first 150 years (van Westen et al., 2018).

In Figure 1a, the standard deviation of the model SSH field in the KCS region is plotted over the model years 250 – 275 (26 years) and is compared to the standard deviation field of the monthly averaged SSH from AVISO
5 (https://www.aviso.altimetry.fr/) over the years 1993 – 2018 in Figure 1b (also 26 years). Overall, both the pattern and amplitude compare reasonably well, but the model overestimates the variability south of Japan compared to observations. In CESM, the KE path is based on the 70-cm SSH contour in the region along 140°E – 160°E and its variations are shown for two specific model years in Figure 1c. The time series of the KE path length is shown in Figure 1e. The red curve is the 36-months running mean of the path length time series and clearly displays decadal time scale variability. Compared to the
10 similarly computed AVISO path variations (Figure 1d), based on the 100-cm SSH contour, and the time series of its path length (Figure 1f) over the period 1993 – 2018, the amplitude and time scale of the variations is well simulated in CESM. The results in Figure 1 show that, although the model forcing is fixed at year 2000 values, the KE path variability and the overall levels of SSH variability are well captured and hence the model appears to be fit for purpose to study the processes controlling the path variability in the KCS.

15 ## 2.2 Phase synchronisation analysis

Phase synchronisation in chaotic oscillators was introduced by Rosenblum et al. (1996) and is extensively described in the book of Pikovsky et al. (2001). While phase synchronisation is often defined as the locking of phases for the case of periodic self-sustained oscillators, a bounded phase difference can also occur in the case of chaotic oscillators (Osipov et al., 2003). Synchronisation of phases has been assessed using different methods (Quiroga et al., 2002; Boccaletti et al., 2001) in a wide
20 range of applications, for example in the climate system (Maraun and Kurths, 2005; Jajcay et al., 2018; Gelbrecht et al., 2018; Paluš and Novotná, 2006; Feliks et al., 2010), in ecology (Blasius et al., 1999), and in physiology such as the cardiorespiratory system (Bartsch et al., 2007; Schäfer et al., 1999).

In order to detect epochs of synchronisation in the KCS we have to choose two time series representing the processes which are supposed to synchronise. For the KE variability, we choose the KE path length time series, as plotted in Figure 1e but
25 then over the full 150 year period (cf. Figure 2c below). This time series was smoothed by a running mean of 36 months and was normalised by its standard deviation. The zonal wind-stress anomaly field over the North Pacific (20°N – 50°N × 100°E – 260°E) was taken as representative for generating the Rossby waves affecting the KCS. Each time series of this field was linearly detrended, the seasonal cycle was removed and then it was normalised by its standard deviation. The resulting time series was then scaled by the area of the grid cell with respect to the largest grid cell area (which is set to 1) and are
30 then processed by Principle Component Analysis (Preisendorfer, 1988). The time series corresponding to the first Principal Component (PC) is used for further analysis (cf. Figure 2d below). This PC time series was also smoothed by a running mean of 36 months and normalised by its standard deviation.

A common approach to derive the phase from a scalar time series $x(t)$ is a two-dimensional embedding by calculating the analytic signal (Gabor, 1946) using the Hilbert transform. First, the time derivative $\dot{x}(t)$ is calculated using a second order
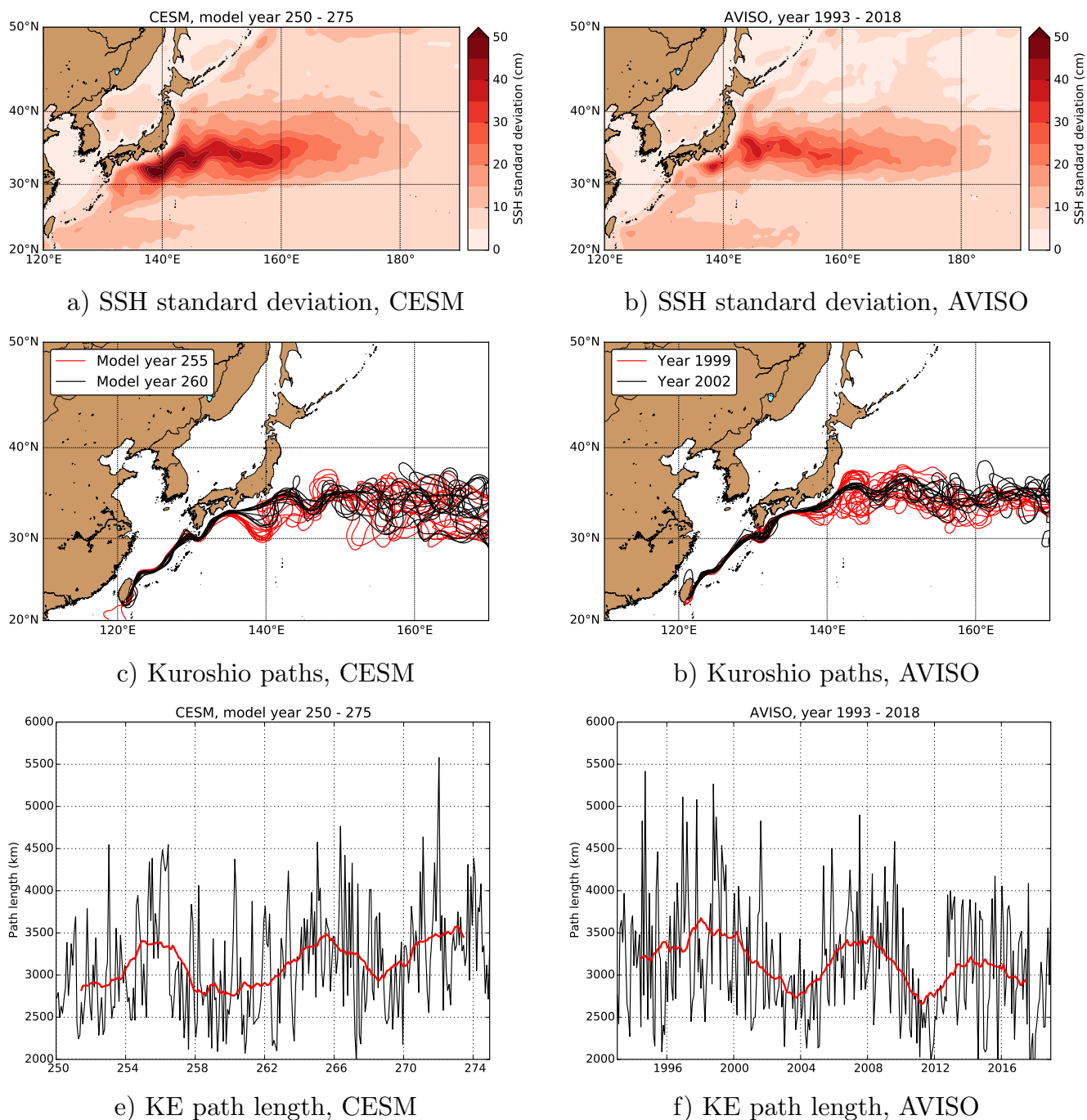
Figure 1. (a): Standard deviation of the SSH field over model years 250 – 275 in CESM. (b): Same for SSH field in the AVISO data over the period 1993 – 2018. (c & d): Monthly mean paths of the Kuroshio for two specific years in CESM and AVISO. (e): Path length of the KE in CESM as determined through the 70-cm SSH contour along the region $140°E – 160°E$. (f): Path length of the KE in AVISO data, similarly computed as for CESM, but using the 100-cm SSH contour. In e) and f), the red curves are the 36-months running mean of the original time series.

differencing scheme to centre the oscillations around the origin and to assure correct phase detection (Osipov et al., 2003). The instantaneous phase in the two dimensional embedding of the signal is then given by:

$$\phi(t) = \arctan\left(\frac{H(\dot{x}(t))}{\dot{x}(t)}\right) \tag{1}$$

where $H(\dot{x}(t))$ is the Hilbert transform of the time derivative $\dot{x}(t)$. Subsequently, the phase difference of two time series $x_i(t)$

5   and $x_j(t)$ is calculated as

$$\Delta\phi(t) = \phi_i(t) - \phi_j(t) \tag{2}$$

Other methods and measures of phase relationship have been used such as the Shannon entropy (Paluš et al., 2007) and the mean resultant length (Paluš et al., 2007). Vejmelka et al. (2009) propose a test that involves the gradient of the phase difference evolution. The quantity of mutual information (Jajcay et al., 2018; Paluš, 2014a, b) serves as an approach to investigate phase

10   synchronisation which is not based on the phase difference evolution and possible plateaus. In addition, other possibilities than the analytic signal Gabor (1946) method exist to derive the instantaneous phase such as the wavelet transform (Paluš and Novotná, 2006).

Epochs of phase synchronization appear as plateaus in the phase difference curve. To avoid a selection of plateaus in the phase difference evolution purely based on visual inspection, we follow Gelbrecht et al. (2018) who provided a statistical

15   test. First, sliding windows of different lengths were applied to compute the phase differences $\Delta\phi(t)$ and for each window the phase difference was mapped back to the interval $[0, 2\pi]$. The distribution of these 'mapped-back' phase differences was then calculated using a histogram with 16 bins. A peak in the distribution of these phase differences then indicates a phase synchronisation while a uniform distribution will result from phases of variables having no relation to each other.

In the results below, 1000 iterative amplitude adjusted Fourier transform (iAAFT) surrogates (Schreiber and Schmitz, 1996)

20   have been generated to test the significance of possible peaks in the histograms. We calculated the k-th surrogate phase difference as (Gelbrecht et al., 2018)

$$\Delta\phi_k^{(s)_k}(t) = \frac{1}{2}\left(\left(\phi_i(t) - \phi_j^{(s)_k}(t)\right) + \left(\phi_i^{(s)_k}(t) - \phi_j(t)\right)\right) \tag{3}$$

where the $(s)_k$ refers to the surrogates. The phase difference distribution of the actual data was then compared to the phase difference distribution of the surrogates using a Kolmogorov-Smirnov (KS) test, with a uniform distribution as a null hypothesis

25   of no-synchronisation. A low p-value ($p < 0.0001$) indicates a rejection of the null hypothesis.

3   Results

We first show a brief model - observation comparison in Section 3.1 to further demonstrate that the model is fit for purpose to analyse KCS path variability. Next, the main results of the paper are provided in Section 3.2, where the phase synchronisation is studied, and in Section 3.3 where the phase synchronisation mechanism is analysed.

Ocean Science
Discussions

3.1 Variability

Figure 2a shows the monthly mean SSH field for January of model year 250 with the 70-cm SSH isoline in black. For the displayed model month, the Kuroshio Current meanders offshore and returns to the coast at approximately 35°N. Here the Kuroshio separates from the coast, forming the meandering eastward flowing KE into the open ocean. The first EOF of the basin wide zonal wind stress (Figure 2b) accounts for 29.6% of the total variance and resembles that of the observed PDO pattern (Deser et al., 2010). Figures 2c and 2d show the KE path length along the region 140°E – 160°E as well as the first PC of the zonal wind stress over the North Pacific basin (100°E – 260°E × 20°N – 50°N).

Before determining the Fourier spectrum, each of the time series is linearly detrended and the seasonal cycle is removed. Surrogate red-noise (2000 realisations) is generated to determine the confidence levels; note that for the wind-stress the lag 1-autocorrelation is small, resulting in effectively white-noise surrogates. Figures 3a – b show the Fourier spectra for the two time series and both display significant (with respect to red noise) decadal variability. Although there is a multi-decadal component of 25 year, a broad range of variability is visible in the 8 – 12 years window. The dominant period of the first PC of the zonal wind stress is 8 years. The spectra using the smoothed time series (using the moving average of 36 months, red curves in Figure 2) also resulted in dominant and significant (> 99% confidence level) periods varying between 7 – 11 years for the KE path length and an 8-year period for the first PC of the zonal wind stress (not shown here).

Motivated by the phase synchronisation studies of Gelbrecht et al. (2018), Feliks et al. (2010) and Paluš and Novotná (2006), a Singular Spectrum Analysis (SSA, Ghil et al. (2002)) was applied to the time series of the KE path length and the first PC of the zonal wind stress to extract significant oscillatory components. Before applying the SSA, the monthly averaged time series are smoothed by a running mean of 36 months. Next, the mean over the smoothed time series was subtracted and the time series was normalised by its standard deviation. The time lag M in the SSA was varied between 250 – 400 months. A Monte Carlo SSA (Allen and Robertson, 1996; Allen and Smith, 1996) was used to test the significance of the components filtered out from each time series against red noise as null hypothesis. Confidence intervals were calculated using 2500 surrogate realisations.

Periods of about 80 – 100 months (7 – 8 years) were found to be significant in both time series in the data basis as well as in the noise basis (Figure 3c – f). The so-called ST-PCs corresponding to the SSA modes for a $M = 365$ months have been used here but we have tested their robustness using various lag-window lengths M between 250 – 400 months. For most M, the ST-PCs that are related to this 7 – 8-year period are between the seventh and ninth ST-PC for the KE path length. For the zonal wind stress, the first two ST-PCs are related to this 7 – 8-year period. These ST-PCs pairs are used to determine the reconstructed components (RCs) and the time series of these RCs are indicated by $L_M(t)$ for the KE path length and $\tau_M^x(t)$ for the zonal wind stress, where the dependence on the lag M is made explicit. These time series will be used in the phase synchronisation analysis described in the following section.

3.2 Phase Synchronisation

The two-dimensional embedding of the derivative of the observables with its Hilbert transform is shown in Figure 4a and 4b for $L_M(t)$ (KE path length) and $\tau_M^x(t)$ (zonal wind stress), respectively for $M = 365$ months. The trajectory in the plane
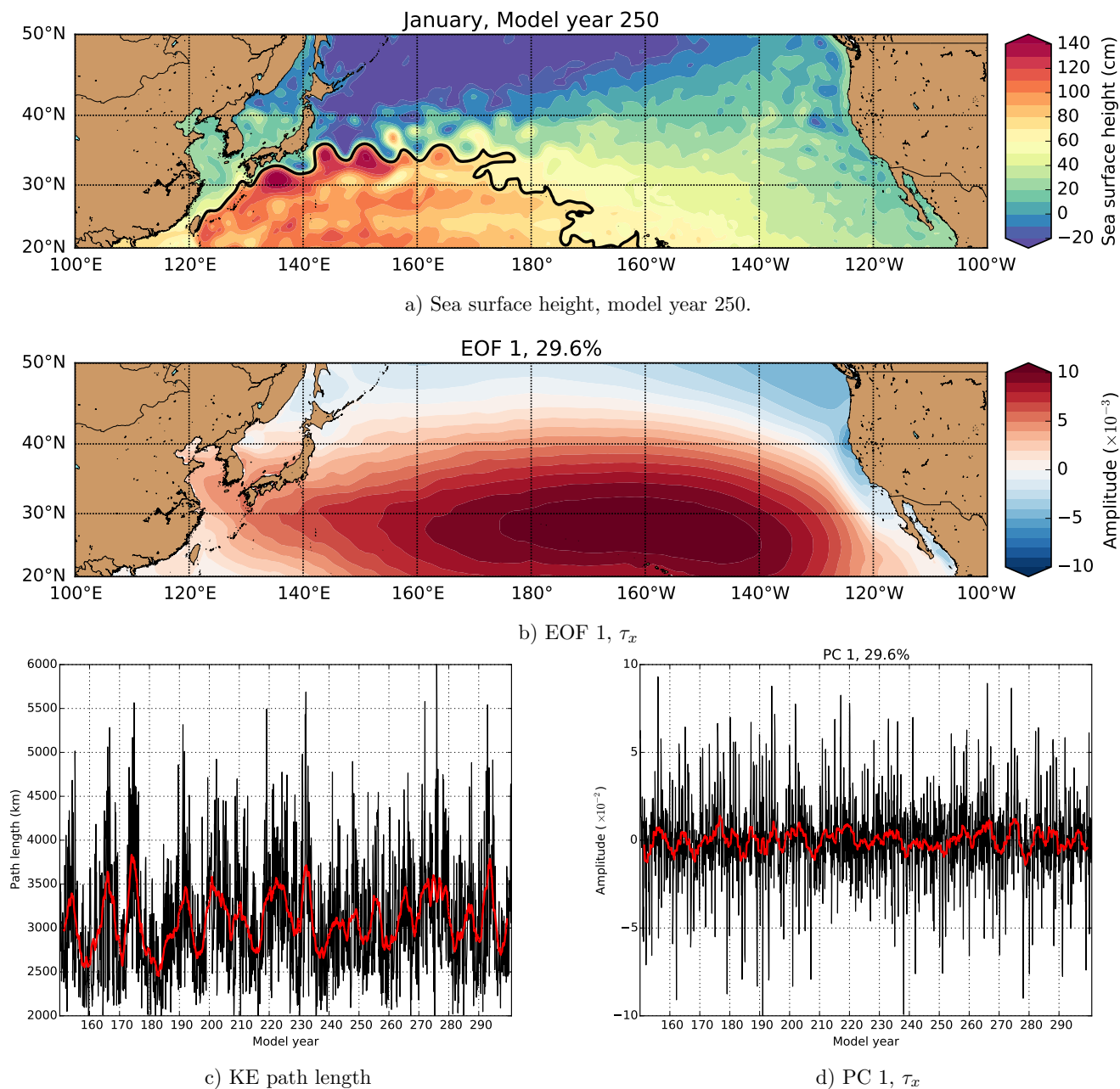
a) Sea surface height, model year 250.

b) EOF 1, τ_x

c) KE path length

d) PC 1, τ_x

Figure 2. (a): Sea surface height field in the North Pacific basin for January model year 250. The black curve is the 70 cm SSH isoline that represents the KE jet. (b): First EOF of the zonal wind stress field over the North Pacific basin ($20°N - 50°N \times 100°E - 260°E$), explaining 29.2 % of the total variance. (c): Time series of the KE path length along the region $140°E - 160°E$, together with its moving average of 36 months (red curve). The path length is derived from the 70 cm SSH isoline, which can be identified in (a). (d): First PC of the zonal wind stress field over the North Pacific basin ($20°N - 50°N \times 100°E - 260°E$), together with its moving average of 36 months (red curve).
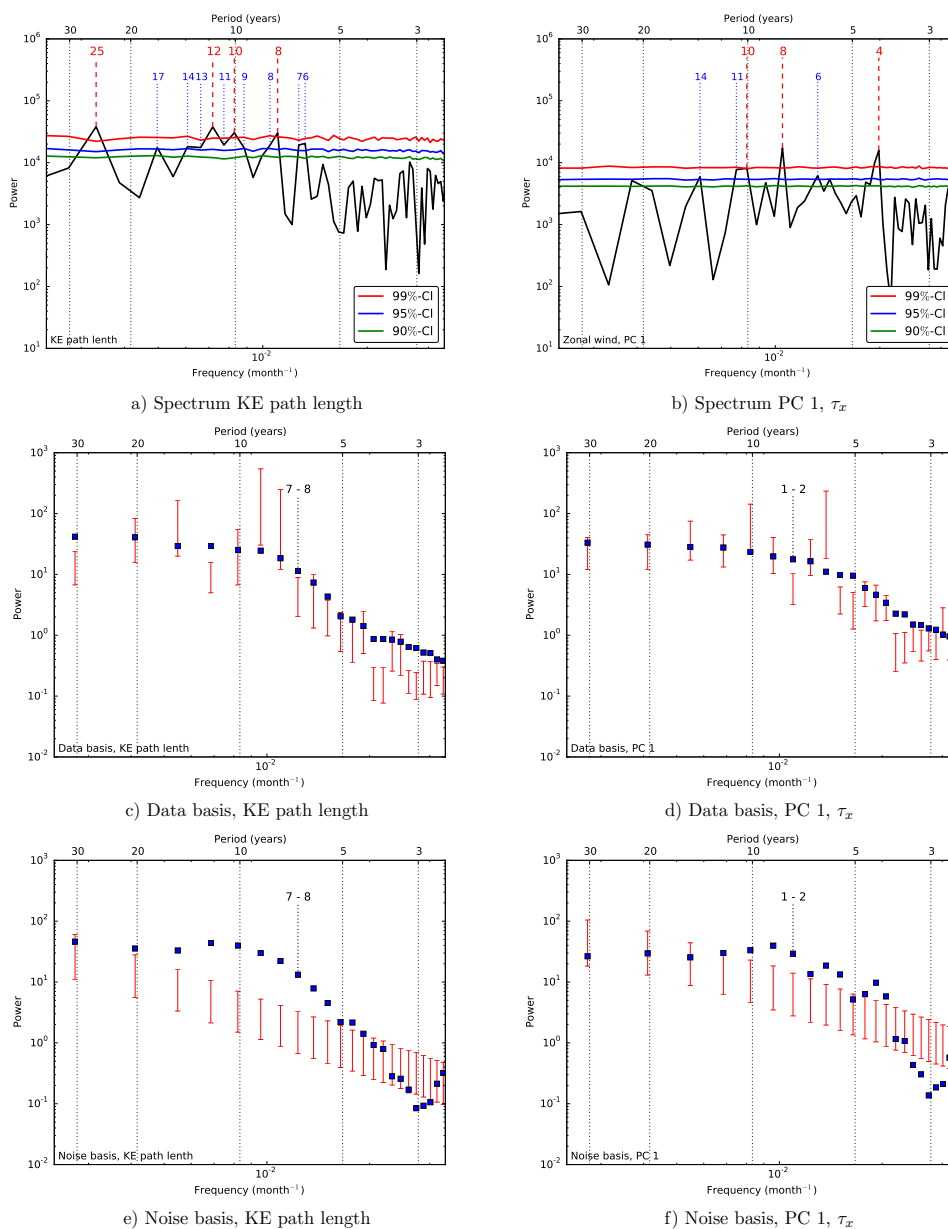
Figure 3. (a & b): Fourier spectrum (black curve) of the KE path length and the first PC of the zonal wind stress. The colour-coded curves are the significance levels of red-noise surrogates, where the numbers (in years) indicate significant periods. (c & d): Data basis from the Monte Carlo SSA for the KE path length and the PC of the zonal wind stress. (e & f): Noise basis from the Monte Carlo SSA for the KE path length and the PC of the zonal wind stress. SSA was performed with a total lag of 365 months and for the Monte Carlo SSA 2500 realisations have been used. The 95% confidence intervals which have been calculated from the surrogates are shown by the red vertical bars. A specific PC is represented by the blue markers and is associated with a certain frequency. The PCs related to the 8-year period are significant in both the data basis and the noise basis (Allen and Robertson, 1996) and the ST-PC pair related to this variability is indicated.

spanned by the time derivative of the observable and its Hilbert transform oscillates a few times around the origin so that the definition of the phase is meaningful and the instantaneous phase can be detected reliably. Note that the multi-centennial length of the model simulation and the SSA filtering is crucial to obtain a clear phase signal. Figure 4c shows the phase difference evolution between $L_M(t)$ and $\tau_M^x(t)$ for three lag-window lengths ($M = 275$, 325 and 365 months). A (significant) plateau

5   can be identified between model year 200 and 240 for all three values of M indicating a phase synchronisation between the time series.

Epochs where plateaus in the phase difference occur are confirmed by the statistical test described in Section 2.2 using a sliding window of 120 months length (Figure 4d). In this figure, p-values smaller than 0.0001 for each M in the KS test allow to reject the null hypothesis related to the uniform distribution of the phase differences. The variation with M shows

10   that phase synchronisation occurs for other values of M as well (Figure 4d). Some window lengths show also a plateau from model year 190 till model year 290. Note that for some lag-window lengths (for example M = 300 – 320) we did not find an appropriate ST-PC pair which is related to the 7 – 8-year oscillation in the SSA.

By processing the model output data by SSA as in Gelbrecht et al. (2018), certain oscillatory components are filtered out and the phase synchronisation analysis is carried out with narrow band signals. This type of data processing introduces a risk

15   of observing plateaus in the phase difference evolution which are interpreted as phase synchronisation but can be technically due to the similarity in the frequencies of the used signals (Paluš and Novotná, 2006). However, here the Fourier spectra of the time series (cf. Figure 3) show dominant periods of about 8 years for the KE path length and the zonal wind stress which are both significant on a 95% significance level. In addition, there is a good physical picture of the coupling between the two time series which is induced by Rossby waves (cf. Section 3.3). More general approaches to study the coupling between the time

20   series can be found in Feliks et al. (2010) and Paluš and Novotná (2006).

We also analysed phase synchronisation in the CESM between the NPGO index (Di Lorenzo et al., 2008) and the KE path length using the same procedure as above. Using the KS-test, we found that there are intervals after model year 220 which significantly differ from the uniform distribution (not shown here). However, after visual inspection (which is of course a subjective measure), these epochs showed no clear plateau compared to those in Figure 4c. In addition, the dominant period

25   of the NPGO index in the CESM output is about 19 years (95%-confidence level). Therefore it is not very likely that phase synchronisation occurs since the spectra of the KE path length shows a dominant period of about 10 years.

Finally, it should be noted that by applying a phase synchronisation analysis and by revealing a dependence between the phases of the observables, synchronisation cannot be deduced unconditionally. Two time series can fulfill the 'mathematical' condition of phase synchronisation which is given by the boundedness of the phase difference even if the observed state arises

30   from other processes or effects (Rosenblum et al., 2001; Vejmelka et al., 2009). Hence, it is critical to also have a physical picture on how this synchronization is established.

3.3   Physical mechanism of phase synchronisation

Self-sustained oscillators synchronise through a coupling which allows the adjustment of the phases. Assessing the processes responsible for the synchronisation is an important but also difficult task, especially for phase synchronisation detected from

a) KE path length

b) PC 1, τ_x

c) Phase difference

d) KS-test, p-value
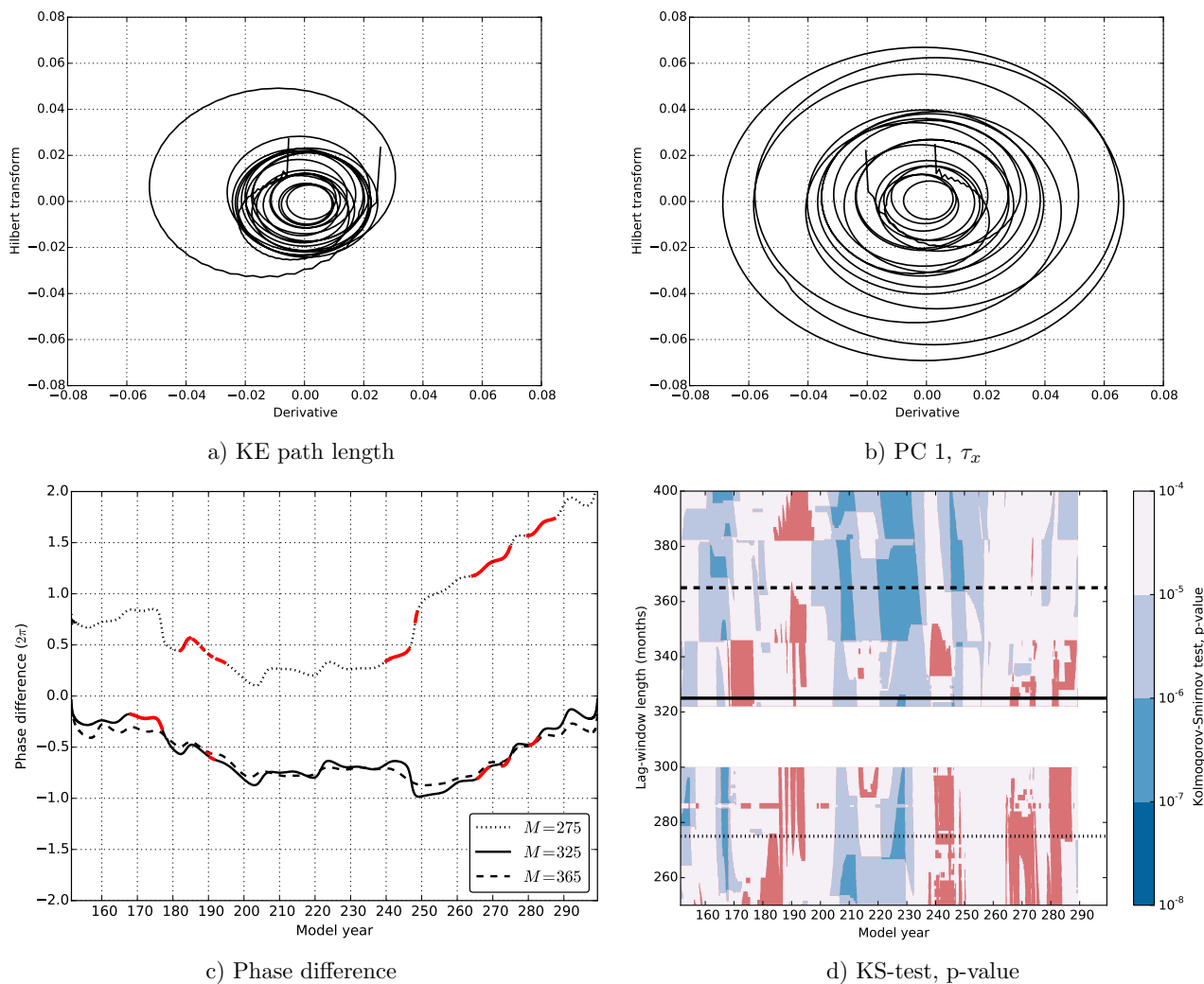
Figure 4. (a & b): Embedding of the time derivative of the KE path length time series $L_M(t)$ (a) and that of the first PC of the zonal wind stress $\tau^x_M(t)$ (b) by the Hilbert transformation. (c): Phase difference between $L_M(t)$ and $\tau^x_M(t)$ for three lag-window lengths M. The black curves indicate starting points of the sliding window (length of 120 months) with p-value < 0.0001. Intervals that are not significant (p-value ≥ 0.0001) are indicated in red. (d): Significance of the phase difference for various lag-window lengths. Regions that are not significant (p-value ≥ 0.0001) are indicated in red. The black horizontal lines indicate the values of M used in (c).

a) SSH Hovmöller   b) IPD Hovmöller

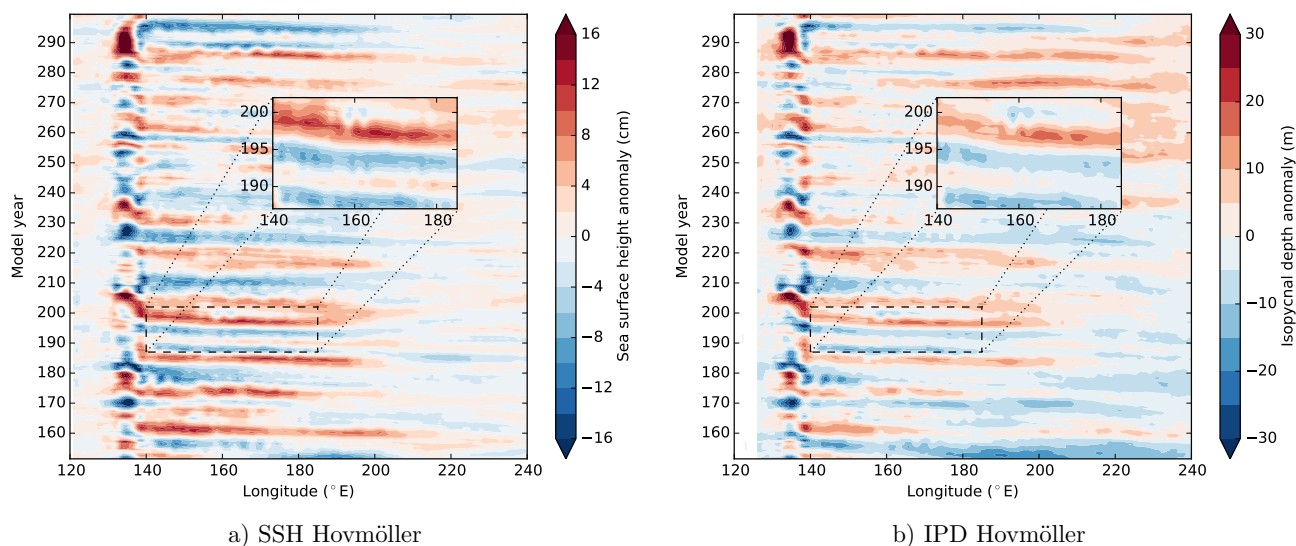**Figure 5.** Hovmöller diagrams of a) SSH anomalies and b) IPD anomalies averaged over $28°N - 30°N$. The result is smoothed by a running mean of 36 months. Positive (Negative) anomalies in the IPD means a deeper (shallower) isopycnal compared to the time-mean. The inset emphasises the (westward) propagation of the anomalies.

data. A good assessment is therefore preferably in an 'experimental setup' where parameters can be varied (Rosenblum et al., 2001; Vejmelka et al., 2009). Formally, the performed phase synchronisation analysis does not allow to infer a direction of coupling between the proposed oscillators. Causality methods as conditional mutual information (Jajcay et al., 2018) or causal discovery algorithms (Schleussner et al., 2014; Runge et al., 2014, 2015) as well as quantifying the direction of influence

5   (Feliks et al., 2010) between the proposed oscillators might help to reveal the direction of coupling.

However, as also mentioned above, here an adequate view on the physics of the system motivates to explore a possible coupling mechanism from the zonal wind stress to the KE path length through the propagation of SSH anomalies. We specifically also focus on the propagation of the anomalies of the depth of the 1028 kg m^{-3} isopycnal, below indicated by the IPD. First, the SSH and IPD anomalies across the basin ($120°E - 240°E$) were averaged along latitude bands, the time-mean was

10   subtracted and the resulting anomalies were smoothed by a running mean of 36 months. The Hovmöller diagrams of the SSH and IPD anomalies averaged over the more southern latitude band of $28°N - 30°N$ (Figure 5) show a westward propagation of the SSH and IPD anomalies starting from the eastern part of the basin and arriving in the KCS. The travel time of these Rossby waves from the eastern to the western side of the North Pacific basin is estimated to be roughly 10 years corresponding to the observed decadal variability of the Kuroshio oscillator. We also find Rossby waves for the more northward latitude bands

15   (tested between $30°N - 34°N$) but the propagation is less clear than in Figure 5 because of the large variability in the KCS.

The Hovmöller diagrams (Figure 5) also indicate that positive (negative) SSH anomalies coincide with positive (negative) IPD anomalies. The stretching of the layer bounded by the surface and the 1028 kg m^{-3} isopycnal, which is on average roughly

12

a) KE path length, IPD and EKE
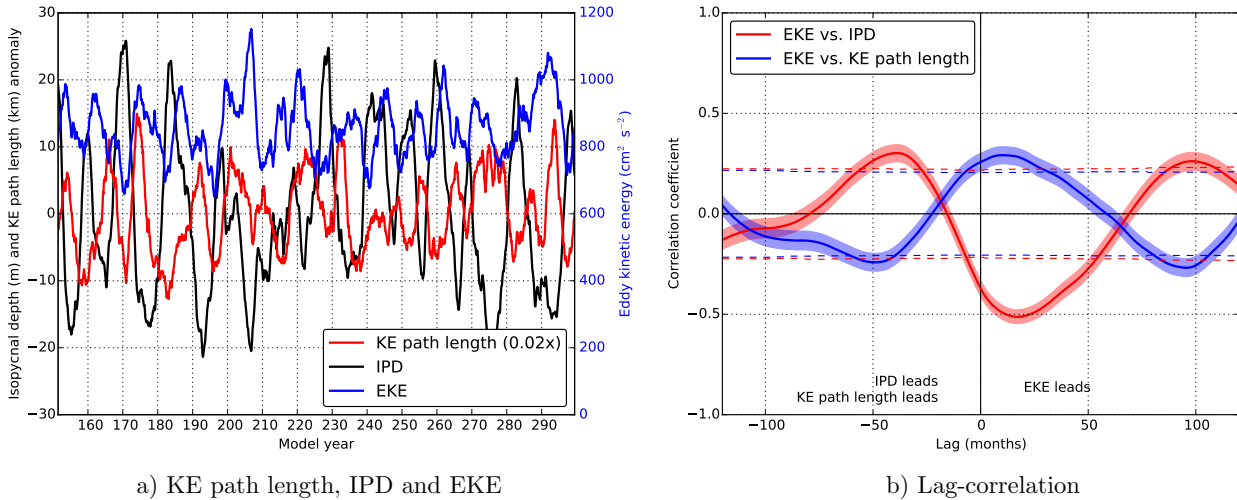
b) Lag-correlation

Figure 6. (a): Time series of SSH, IPD and EKE. The time-mean is subtracted to retain anomalies for the SSH and IPD time series. All time series are smoothed by a running mean of 36 months. (b): EKE and the time derivative of the IPD, retained from the smoothed time series. (c): Lag-correlation between the IPD, SSH and EKE time series. The shading indicates the 95%-confidence interval and the dashed curves indicate significant correlations (95%-confidence level.) (d): Same as c), but now for the time derivative IPD and EKE.

500 m deep in this region, leads to variability in the horizontal velocity field which will affect instabilities of the KCS. We next analysed the eddy kinetic energy (EKE) and IPD over the whole KCS area to study the connection between IPD variation and EKE. The local EKE is here defined as

$$\text{EKE} = \frac{1}{2}\left((u - \bar{u})^2 + (v - \bar{v})^2\right) \tag{4}$$

5   where u and v are the local monthly-averaged zonal and meridional velocity, respectively and $\bar{u}$ and $\bar{v}$ are their time mean.

    The quantities EKE and IPD are averaged over $30°\text{N} - 35°\text{N}$ and $135°\text{E} - 145°\text{E}$, and the EKE is additionally averaged over the upper 500 m. For this averaged IPD and the KE path length (as in Figure 2c), the time-mean is subtracted; the three time series (EKE, IPD and KE path length) are smoothed with a running mean of 36 months and plotted in Figure 6a. The time series for IPD and EKE are clearly out of phase, and the IPD appears to lead the EKE by about 40 months (Figure 6b).

10 The highest lag-correlation (0.29, significant at 95%-Cl) between EKE and KE path length is +10 months, with EKE leading (Figure 6b). However, taking the spatial average over a larger region (for example, $30°\text{N} - 35°\text{N} \times 140°\text{E} - 160°\text{E}$) for the EKE resulted in higher lag-correlation coefficients with the KE path length.

    Although, due to the periodicity, it is not entirely clear which time series leads or lags, we can interpret the results in Figure 6 as follows. During the deepening of the IPD (positive values), the overall velocity field decreases which leads to a weaker

15 flow in the upper layer (defined by the IPD). Hence, there is a decreased growth rate of barotropic instabilities, which leads to relative low values of EKE. The optimal lag-correlation his expected to occur at about 1/2 of the mean oscillation period, which is about 4 years, consistent with Figure 6b. A low (high) degree of instability growth also leads a long (short) KE path length

and is hence associated with an elongated (contracted) state of the KE. This view is also compatible with the analysis of other results in OGCMs (Taguchi et al., 2005, 2010) indicating that the Rossby waves can 'trigger' the frontal (internal) instabilities.

4   Summary, Discussion and Conclusions

Output from a multi-centennial simulation with a high-resolution version of the Community Climate System Model (CESM)
5   was used to study phase synchronisation between path variability in the Kuroshio Current System (KCS) and the wind variability over the North Pacific basin. In particular, by performing an SSA, oscillatory components on decadal scales of the Kuroshio Extension (KE) path length and the first PC of the zonal wind-stress field were chosen as representative observables for the proposed oscillators. The length of the CESM simulation is crucial for determining an adequate phase of the KE path length and the zonal wind-stress variability. The high spatial resolution of the ocean model component is also needed to adequately
10   represent the internal variability in the KCS. The phase difference evolution, the distributions of the phase difference and results from a statistical test indicate that the KE and the North Pacific zonal wind stress are episodically phase synchronised in CESM.

We interpret this phase synchronisation as an entrainment of an 'external' frequency (that of the mid-basin wind stress variability) into the variability of a chaotic system (the KCS), as described in section 5.2 of Pikovsky et al. (2001). Although
15   there are effects of variations of the KSC on the atmospheric circulation (predominantly local) as for example described in Qiu et al. (2014), there is ample evidence that the PDO and/or NPGO variability is independent of the KCS as it is also found in low-resolution ocean/coupled models (Weijer et al., 2013). Hence, the wind-stress variability acts as a forcing on the Rossby waves which couple to the KCS system through the motion of isopycnals as shown in Section 3.3.

When this forcing is too large, the period of the 'external' frequency is dominant and hence the resulting KCS would be
20   periodic, which it is clearly not. When the forcing is too small, phase diffusion induced by nonlinearities in the KCS would be dominant and prevent phase synchronisation. This likely explains why only during a few intervals, the phases are synchronised. The IPD amplitude becomes large (negative) just (Figure 6a) before the synchronisation interval (model years 200 – 240) and when its amplitude drops again (model years 240 – 250), phase synchronisation disappears. Hence, the variation in the forcing sets the epochs of the phase synchronisation.

25   We think that the phase synchronisation, together with its mechanism as described in Section 3.3, provides a missing piece in the puzzle connecting the purely Rossby wave 'forced' view of KCS path transitions, as originally advocated (Qiu and Chen, 2005, 2010) and the pure internal variability view (Pierini et al., 2009; Berloff et al., 2007). In the model world of CESM, the Rossby waves are clearly required to obtain a very pronounced decadal variability. This view is supported by (not shown) results we obtained with an OGCM-only (the POP model) which was forced by a seasonal cycle (for the simulation details,
30   see Weijer et al. (2012)). While transitions between the different KE states occur regularly in the CESM output, they develop more randomly in the POP simulation because there can be no phase synchronisation.

Indications that some periods of observed variability show a much clearer decadal variability than others are found in the analysis of AVISO data (Gentile et al., 2018). However, one cannot detect the phase synchronisation from observations yet

as the AVISO time series of SSH is too short. Analysis of a 26-year interval (out of the 150 year total interval) of CESM output indicated that (with a period of variability of about 8 years), it is not possible to detect such a phase synchronisation. Unfortunately, we will have to accept that we will have to wait for a few (about 5 – 6) decades before this phenomenon can be demonstrated from accurate observational data.

Ocean Science
Discussions

Open Access

EGU

References

Allen, M. and Robertson, A.: Distinguishing modulated oscillations from coloured noise in multivariate datasets, Climate dynamics, 12, 775–784, 1996.

Allen, M. R. and Smith, L. A.: Monte Carlo SSA: Detecting irregular oscillations in the presence of colored noise, Journal of climate, 9, 3373–3404, 1996.

Bartsch, R., Kantelhardt, J. W., Penzel, T., and Havlin, S.: Experimental evidence for phase synchronization transitions in the human cardiorespiratory system, Physical review letters, 98, 054 102, 2007.

Berloff, P. S., Hogg, A. M., and Dewar, W. K.: The turbulent oscillator: a mechanism of low-frequency variability of the wind-driven ocean gyres, Journal Of Physical Oceanography, 37, 2362–2386, 2007.

Blasius, B., Huppert, A., and Stone, L.: Complex dynamics and phase synchronization in spatially extended ecological systems, Nature, 399, 354, 1999.

Boccaletti, S., Pecora, L. M., and Pelaez, A.: Unifying framework for synchronization of coupled dynamical systems, Physical Review E, 63, 066 219, 2001.

Ceballos, L. I., Di Lorenzo, E., Hoyos, C. D., Schneider, N., and Taguchi, B.: North Pacific Gyre Oscillation synchronizes climate fluctuations in the eastern and western boundary systems, Journal of Climate, 22, 5163–5174, 2009.

Deser, C., Alexander, M. A., and Timlin, M. S.: Evidence for a wind-driven intensification of the Kuroshio Current Extension from the 1970s to the 1980s, Journal of Climate, 12, 1697–1706, 1999.

Deser, C., Alexander, M. a., Xie, S.-P., and Phillips, A. S.: Sea Surface Temperature Variability: Patterns and Mechanisms, Annual Review of Marine Science, 2, 115–143, 2010.

Di Lorenzo, E., Schneider, N., Cobb, K. M., Franks, P., Chhak, K., Miller, A. J., McWilliams, J. C., Bograd, S. J., Arango, H., Curchitser, E., et al.: North Pacific Gyre Oscillation links ocean climate and ecosystem change, Geophysical Research Letters, 35, 2008.

Feliks, Y., Ghil, M., and Robertson, A. W.: Oscillatory climate modes in the Eastern Mediterranean and their synchronization with the North Atlantic Oscillation, Journal of Climate, 23, 4060–4079, 2010.

Gabor, D.: Theory of communication. Part 1: The analysis of information, Journal of the Institution of Electrical Engineers-Part III: Radio and Communication Engineering, 93, 429–441, 1946.

Gelbrecht, M., Boers, N., and Kurths, J.: Phase coherence between precipitation in South America and Rossby waves, Science advances, 4, eaau3191, 2018.

Gentile, V., Pierini, S., de Ruggiero, P., and Pietranera, L.: Ocean modelling and altimeter data reveal the possible occurrence of intrinsic low-frequency variability of the Kuroshio Extension, Ocean Modelling, 131, 24–39, 2018.

Ghil, M., Allen, M. R., Dettinger, M. D., Ide, K., Kondrashov, D., Mann, M. E., Robertson, A. W., Saunders, A., Tian, Y., Varadi, F., and Yiou, P.: Advanced spectral methods for climatic time series, Reviews Of Geophysics, 40, 3.1–3.41, 10.1029/2000GR000092, 2002.

Hu, D., Wu, L., Cai, W., Gupta, A. S., Ganachaud, A., Qiu, B., Gordon, A. L., Lin, X., Chen, Z., Hu, S., Wang, G., Wang, Q., Sprintall, J., Qu, T., Kashino, Y., Wang, F., and Kessler, W. S.: Pacific western boundary currents and their roles in climate, Nature, 522, 299–308, 2015.

Jajcay, N., Kravtsov, S., Sugihara, G., Tsonis, A. A., and Paluš, M.: Synchronization and causality across time scales in El Niño Southern Oscillation, npj Climate and Atmospheric Science, 1, 33, 2018.

Ocean Science
Discussions

Open Access

EGU

Kawabe, M.: Variations of Current Path, Velocity, and Volume Transport of the Kuroshio in Relation with the Large Meander, Journal of Physical Oceanography, 25, 3103–3117, doi:10.1175/1520-0485(1995)025<3103:VOCPVA>2.0.CO;2, http://journals.ametsoc.org/doi/abs/10.1175/1520-0485%281995%29025%3C3103%3AVOCPVA%3E2.0.CO%3B2, 1995.

Ma, L.: Response of ocean dynamics to multiple equilibria of the Kuroshio path South of Japan, Dyn. Atm. Oceans, pp. 1–15, 2019.

5 Mantua, N. J., Hare, S. R., Zhang, Y., Wallace, J. M., and Francis, R. C.: A Pacific interdecadal climate oscillation with impacts on salmon production, Bulletin of the american Meteorological Society, 78, 1069–1080, 1997.

Maraun, D. and Kurths, J.: Epochs of phase coherence between El Nino/Southern Oscillation and Indian monsoon, Geophysical Research Letters, 32, 2005.

Munk, W.: On the wind-driven ocean circulation, J. Meteorol., 7, 79–93, 1950.

10 Osipov, G. V., Hu, B., Zhou, C., Ivanchenko, M. V., and Kurths, J.: Three types of transitions to phase synchronization in coupled chaotic oscillators, Physical Review Letters, 91, 024 101, 2003.

Paluš, M.: Multiscale atmospheric dynamics: cross-frequency phase-amplitude coupling in the air temperature, Physical review letters, 112, 078 702, 2014a.

Paluš, M.: Cross-scale interactions and information transfer, Entropy, 16, 5263–5289, 2014b.

15 Paluš, M. and Novotná, D.: Quasi-biennial oscillations extracted from the monthly NAO index and temperature records are phase-synchronized, Nonlinear Processes in Geophysics, 13, 287–296, 2006.

Paluš, M., Kurths, J., Schwarz, U., Seehafer, N., Novotná, D., and Charvátová, I.: The solar activity cycle is weakly synchronized with the solar inertial motion, Physics Letters A, 365, 421–428, 2007.

Penduff, T., Juza, M., Barnier, B., Zika, J., Dewar, W. K., Treguier, A. M., Molines, J.-M., and Audiffren, N.: Sea Level Expression of 20 Intrinsic and Forced Ocean Variabilities at Interannual Time Scales, Journal Of Climate, 24, 5652–5670, 2011.

Pierini, S.: A Kuroshio Extension System Model Study: Decadal Chaotic Self-Sustained Oscillations, Journal of Physical Oceanography, 36, 1605–1625, http://journals.ametsoc.org/doi/abs/10.1175/JPO2931.1, 2006.

Pierini, S.: Kuroshio Extension bimodality and the North Pacific Oscillation: A case of intrinsic variability paced by external forcing, Journal of Climate, 27, 448–454, 2014.

25 Pierini, S., Dijkstra, H. A., and Riccio, A.: A Nonlinear Theory of the Kuroshio Extension Bimodality, Journal of Physical Oceanography, 39, 2212–2229, 2009.

Pikovsky, A., Rosenblum, M., and Kurths, J.: Synchronization, Cambridge University Press, 2001.

Preisendorfer, R. W.: Principal Component Analysis in Meteorology and Oceanography, Elsevier, Amsterdam, The Netherlands, 1988.

Qiu, B.: The Kuroshio Extension system: Its large-scale variability and role in the midlatitude ocean-atmosphere interaction, Journal of 30 Oceanography, 58, 57–75, 2002.

Qiu, B. and Chen, S.: Variability of the Kuroshio Extension Jet, Recirculation Gyre, and Mesoscale Eddies on Decadal Time Scales, Journal of Physical Oceanography, 35, 2090–2103, 2005.

Qiu, B. and Chen, S.: Eddy-mean flow interaction in the decadally modulating Kuroshio Extension system, Deep-Sea Research Part Ii-Topical Studies In Oceanography, 57, 1098–1110, 2010.

35 Qiu, B., Chen, S., Schneider, N., and Taguchi, B.: A Coupled Decadal Prediction of the Dynamic State of the Kuroshio Extension System, Journal Of Climate, 27, 1751–1764, 2014.

Quiroga, R. Q., Kraskov, A., Kreuz, T., and Grassberger, P.: Performance of different synchronization measures in real data: a case study on electroencephalographic signals, Physical Review E, 65, 041 903, 2002.

Rosenblum, M., Pikovsky, A., Kurths, J., Schäfer, C., and Tass, P. A.: Phase synchronization: from theory to data analysis, in: Handbook of biological physics, vol. 4, pp. 279–321, Elsevier, 2001.

Rosenblum, M. G., Pikovsky, A. S., and Kurths, J.: Phase synchronization of chaotic oscillators, Physical review letters, 76, 1804, 1996.

Runge, J., Petoukhov, V., and Kurths, J.: Quantifying the strength and delay of climatic interactions: The ambiguities of cross correlation and a novel measure based on graphical models, Journal of Climate, 27, 720–739, 2014.

Runge, J., Petoukhov, V., Donges, J. F., Hlinka, J., Jajcay, N., Vejmelka, M., Hartman, D., Marwan, N., Paluš, M., and Kurths, J.: Identifying causal gateways and mediators in complex spatio-temporal systems, Nature communications, 6, 8502, 2015.

Schäfer, C., Rosenblum, M. G., Abel, H.-H., and Kurths, J.: Synchronization in the human cardiorespiratory system, Physical Review E, 60, 857, 1999.

Schleussner, C.-F., Runge, J., Lehmann, J., and Levermann, A.: The role of the North Atlantic overturning and deep ocean for multi-decadal global-mean-temperature variability, Earth System Dynamics, 5, 103–115, 2014.

Schmeits, M. J. and Dijkstra, H. A.: Bimodality of the Kuroshio and the Gulf Stream, Journal Of Physical Oceanography, 31, 2971–2985, 2001.

Schreiber, T. and Schmitz, A.: Improved surrogate data for nonlinearity tests, Physical Review Letters, 77, 635, 1996.

Sérazin, G., Penduff, T., Barnier, B., Molines, J.-M., Arbic, B. K., Müller, M., and Terray, L.: Inverse cascades of kinetic energy as a source of intrinsic variability: A global OGCM study, Journal Of Physical Oceanography, 48, 1385–1408, 2018.

Simonnet, E., Dijkstra, H. A., and Ghil, M.: Homoclinic bifurcations in the quasi-geostrophic double-gyre circulation, Journal Of Marine Research, 63, 931–956, 2005.

Speich, S., Dijkstra, H. A., and Ghil, M.: Successive bifurcations of a shallow-water model with applications to the wind driven circulation, Nonlin. Proc. Geophys., 2, 241–268, 1995.

Stommel, H.: The westward intensification of wind-driven ocean currents, Trans. Amer. Geophysical Union, 29, 202–206, 1948.

Sugimoto, S. and Hanawa, K.: Relationship between the path of the Kuroshio in the south of Japan and the path of the Kuroshio Extension in the east, Journal Of Oceanography, 68, 219–225, 2011.

Sverdrup, H. U.: Wind-driven currents in a baroclinic ocean with application to the equatorial current in the eastern Pacific, Proc. Natl. Acad. Sci. Wash., 33, 318–326, 1947.

Taft, B. A.: Characteristics of the flow of the Kuroshio south of Japan, in: Kuroshio, physical aspects of the Japan current, edited by Stommel, H. and Yoshida, K., Univ. Washington Press, Seattle, USA, 1972.

Taguchi, B., Xie, S. P., Mitsudera, H., and Kubokawa, A.: Response of the Kuroshio Extension to Rossby waves associated with the 1970s climate shift in a high resolution ocean model, J Climate, 18, 2979–2995, 2005.

Taguchi, B., Xie, S. P., Schneider, N., Nonaka, M., Sasaki, H., and Sasai, Y.: Decadal variability of the Kuroshio Extension: Observations and an eddy-resolving model hincast, J Climate, 20, 2357–2377, 2007.

Taguchi, B., Nakamura, H., Nonaka, M., and Xie, S.-P.: Influences of the Kuroshio/Oyashio Extensions on Air-Sea Heat Exchanges and Storm-Track Activity as Revealed in Regional Atmospheric Model Simulations for the 2003/04 Cold Season, Journal of Climate, 22, 6536–6560, 2009.

Taguchi, B., Qiu, B., Nonaka, M., Sasaki, H., Xie, S.-P., and Schneider, N.: Decadal variability of the Kuroshio Extension: mesoscale eddies and recirculations, Ocean Dynamics, 60, 673–691, 2010.

Ocean Science
Discussions

Open Access

EGU

van Westen, R. M., Dijkstra, H. A., Klees, R., Riva, R. E. M., Slobbe, D. C., van der Boog, C. G., Katsman, C. A., Candy, A. S., Pietrzak, J. D., Zijlema, M., James, R. K., and Bouma, T. J.: Mechanisms of the 40-70 Day Variability in the Yucatan Channel Volume Transport, Journal Of Geophysical Research-Oceans, 123, 1286–1300, 2018.

Vejmelka, M., Paluš, M., and Lee, W.: Phase synchronization analysis by assessment of the phase difference gradient, Chaos: An Interdisci-

5   plinary Journal of Nonlinear Science, 19, 023 120, 2009.

Wang, S., Liu, Z., Pang, C., and Liu, H.: The decadally modulating eddy field in the upstream Kuroshio Extension and its related mechanisms, Acta Oceanologica Sinica, 35, 9–17, 2016.

Weijer, W., Maltrud, M. E., Hecht, M. W., Dijkstra, H. A., and Kliphuis, M. A.: Response of the Atlantic Ocean circulation to Greenland Ice Sheet melting in a strongly-eddying ocean model, Geophysical Research Letters, 39, 2012.

10   Weijer, W., Muñoz, E., Schneider, N., and Primeau, F.: Pacific Decadal Variability: Paced by Rossby Basin Modes?, Journal Of Climate, 26, 1445–1456, 2013.

Wu, L., Cai, W., Zhang, L., Nakamura, H., Timmermann, A., Joyce, T., McPhaden, M. J., Alexander, M., Qiu, B., Visbeck, M., Chang, P., and Giese, B.: Enhanced warming over the global subtropical western boundary currents, Nature Publishing Group, 2, 161–166, 2012.

Yang, Y., San Liang, X., Qiu, B., and Chen, S.: On the Decadal Variability of the Eddy Kinetic Energy in the Kuroshio Extension, Journal

15   Of Physical Oceanography, 47, 1169–1187, 2017.